

## Supplementary Materials for

# Tuning of anomalous magnetotransport properties in half-Heusler topological semimetal GdPtBi

Orest Pavlosiuk<sup>1,\*</sup>, Piotr Wiśniewski<sup>1</sup>, Romain Grasset<sup>2</sup>, Marcin Konczykowski<sup>2</sup>, Andrzej Ptok<sup>3</sup>, Dariusz Kaczorowski<sup>1,\*</sup>

<sup>1</sup> *Institute of Low Temperature and Structure Research, Polish Academy of Sciences, ul. Okólna 2, 50-422 Wrocław, Poland*

<sup>2</sup> *Laboratoire des Solides Irradiés, École Polytechnique, 91128 Palaiseau, France*

<sup>3</sup> *Institute of Nuclear Physics, Polish Academy of Sciences, W. E. Radzikowskiego 152, PL-31342 Kraków, Poland*

\* *Corresponding authors: d.kaczorowski@intibs.pl, o.pavlosiuk@intibs.pl*

### Magnetoresistance and electrical resistivity of pristine samples

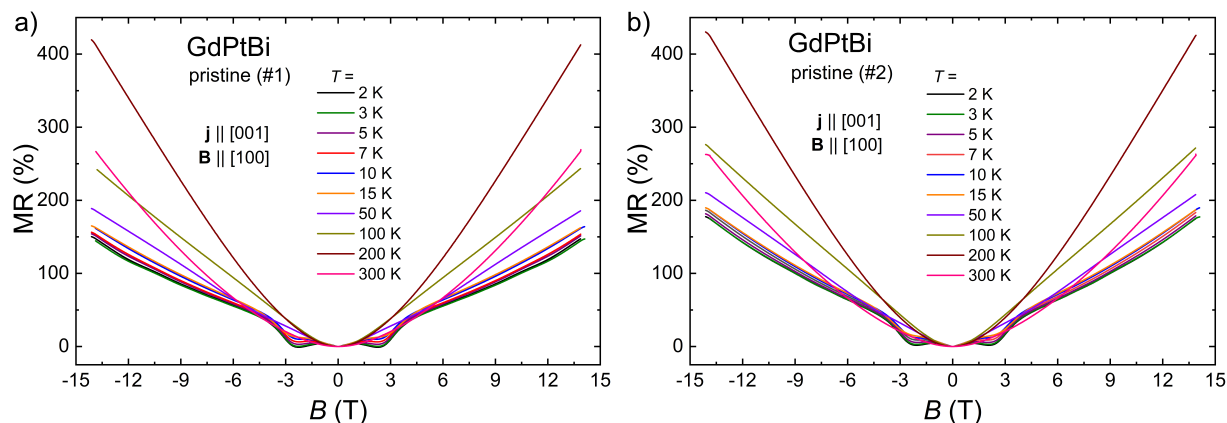


FIG. S1. Magnetoresistance isotherms as a function of magnetic field measured at several different temperatures for pristine sample #1 (a) and pristine sample #2 (b). During the measurements electrical current was applied along [001] crystallographic direction and magnetic field was applied along [100] crystallographic direction.

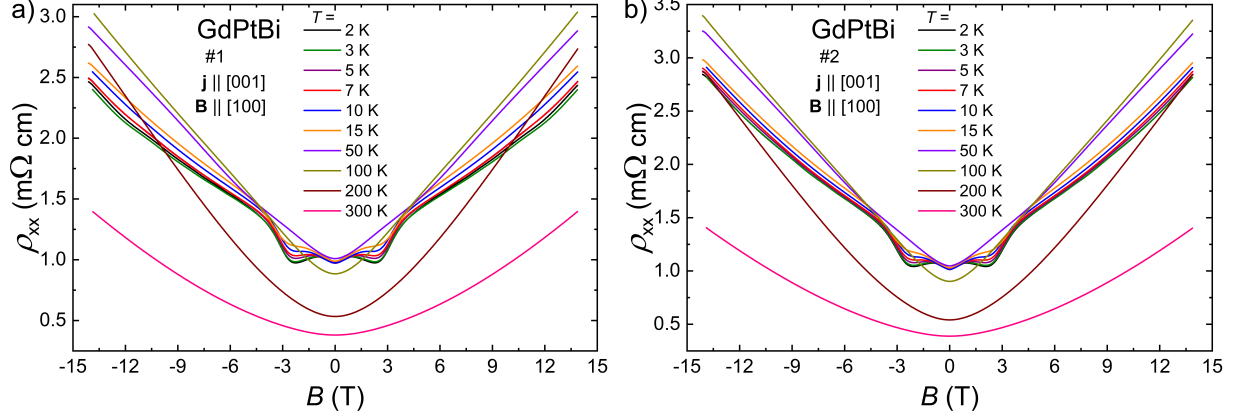


FIG. S2. Electrical resistivity as a function of magnetic field measured at several temperatures for pristine sample #1 (a) and pristine sample #2 (b). During the measurements electrical current was applied along [001] crystallographic direction and magnetic field was applied along [100] crystallographic direction. The data presented in this figure correspond to those shown in Fig. S1.

### Electrical resistivity of all studied samples

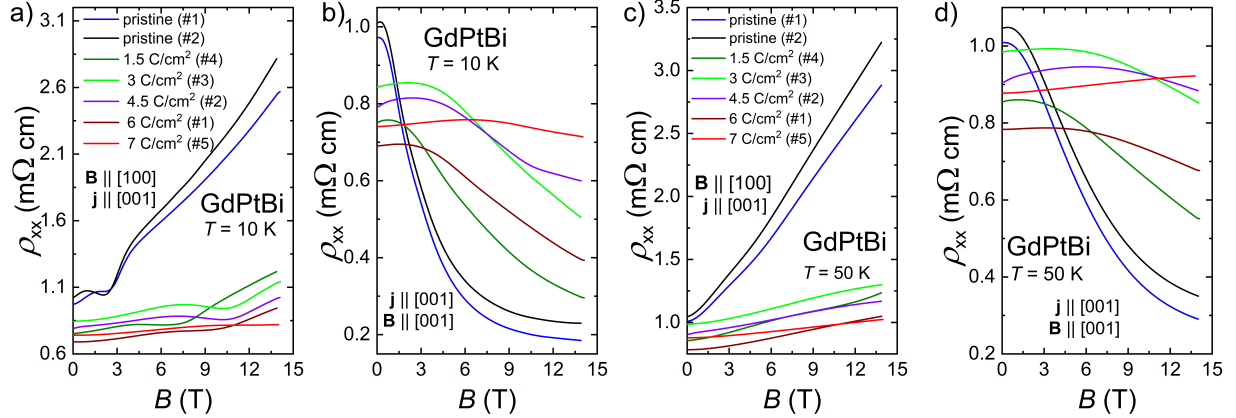


FIG. S3. Magnetic field dependence of the electrical resistivity of all studied samples measured in transverse configuration at  $T = 10$  K (a) and  $T = 50$  K (c). Magnetic field dependence of electrical resistivity of all studied samples measured in longitudinal configuration at  $T = 10$  K (b) and  $T = 50$  K (d). The data presented in this figure correspond to those shown in Fig. 3a,b,e,f in the main text.

## Antisymmetrization and symmetrization of raw magnetotransport data

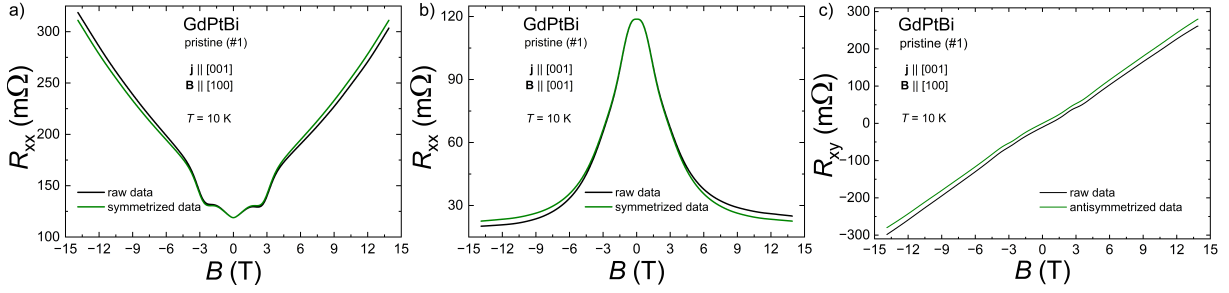


FIG. S4. The magnetic field dependences of the raw data (black lines) and the (anti)symmetrized data (olive lines) of the transverse resistance (a), longitudinal resistance (b) and Hall resistance (c) for the pristine sample #1 of GdPtBi that was measured at  $T = 10$  K.

## Separation of anomalous Hall contribution

The anomalous Hall effect has been observed in a number of half-Heusler compounds.[S1–S7] There are several different approaches that can be taken in order to extract the contribution of AHE to the total Hall effect observed in  $REPtBi$  half-Heusler compounds.[S2–S5] It is evident that  $\sigma_{xy}(B)$  curves obtained at  $T = 10$  K for all studied samples, show an anomaly due to the AHE. Furthermore, this anomaly changes its position with respect to the magnetic field scale (see Fig. S5). In pristine samples, AHE reaches its maximum in the low magnetic field region. In contrast, in irradiated samples, AHE shifts towards a stronger magnetic field. Accordingly, methods based on the fitting of Drude model,[S3, S4] can be hardly applied in our case (see description below). Therefore, we used the approach previously reported for AHE analysis in TbPtBi[S5], which is the most suitable to our data set. In this approach, it has been assumed that at sufficiently high temperatures, AHE can be completely neglected, and the total Hall signal at this particular temperature can be considered to be equal to the ordinary Hall effect contribution at low temperature. A comparison of  $\sigma_{xy}(B)$  isotherms measured in the temperature range 2-300 K revealed that the lowest temperature at which AHE is negligible is 50 K. Furthermore, there is a slight difference between  $\rho_{xy}(B)$  measured at  $T = 10$  K and  $T = 50$  K, therefore it is a good assumption that  $\sigma_{xy}(B)$  at  $T = 50$  K corresponds to the ordinary Hall contribution at  $T = 10$  K. Fig. S5a-f, shows the magnetic field dependence of  $\sigma_{xy}$  at  $T = 10$  K (blue curves)

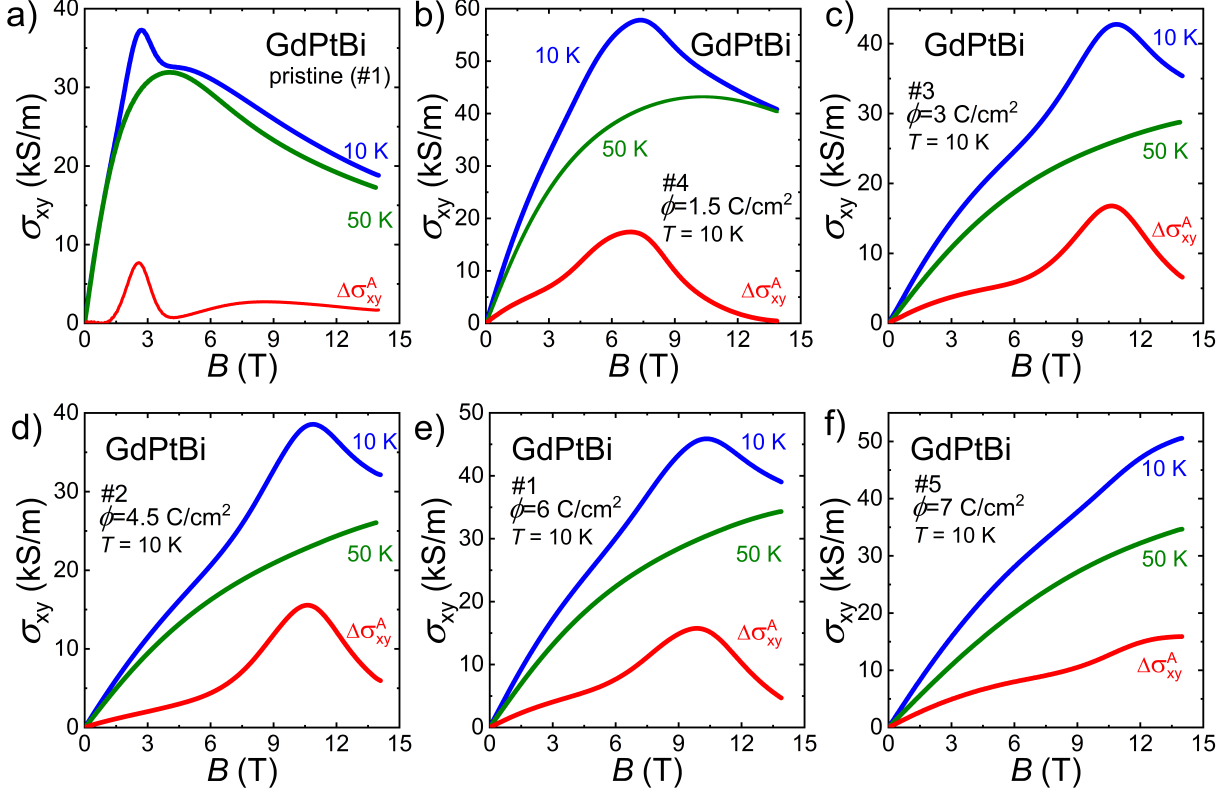


FIG. S5. Separation of anomalous Hall contribution using the approach of subtraction of experimental curves measured at two different temperatures. Magnetic field dependence of Hall conductivity measured at  $T = 10$  K (blue line), at  $T = 50$  K (olive line) and their difference (red line) for pristine sample #1 (a), sample irradiated with  $\phi = 1.5$  C/cm<sup>2</sup> (b),  $\phi = 3$  C/cm<sup>2</sup> (c),  $\phi = 4.5$  C/cm<sup>2</sup> (d),  $\phi = 6$  C/cm<sup>2</sup> (e) and  $\phi = 7$  C/cm<sup>2</sup> (f).

and  $T = 50$  K (olive curves), as well as their difference, which corresponds to AHE ( $\sigma_{xy}^A = \sigma_{xy}(10\text{ K}) - \sigma_{xy}(50\text{ K})$ , red curves) for particular samples.

In the case of our dataset, the AHE extraction approach, which is predicated on the fitting of Hall conductivity to the Drude formula has a salient drawback. Specifically, for different samples, it is necessary to select distinct ranges of magnetic fields for which the Drude model can be applied. This limitation originates from the observation that the position of the anomaly related to AHE on the magnetic field length scale varies from sample to sample. Therefore, it is impossible to select a single range of fitting that would be applicable to all samples. Nevertheless, we employed the aforementioned approach to extract AHE contribution. Initially, experimental data (black points in Fig. S6) within a particular range of magnetic field were fitted with the

single-band Drude model:

$$\sigma_{xy} = \frac{en\mu^2 B}{1 + (\mu B)^2}, \quad (\text{S1})$$

where,  $e$  represents the elementary charge, and  $n$  and  $\mu$  are the carrier concentration and mobility, respectively. Subsequently, the values of the obtained fitted parameters were used to generate theoretical curves (solid olive lines in Fig. S6) for the entire range of magnetic fields that were studied. Finally, the theoretical curve was subtracted from the experimental one, and the obtained difference (red solid curves in Fig. S6) corresponds to the anomalous Hall conductivity (AHC),  $\Delta\sigma_{xy}^A$ .

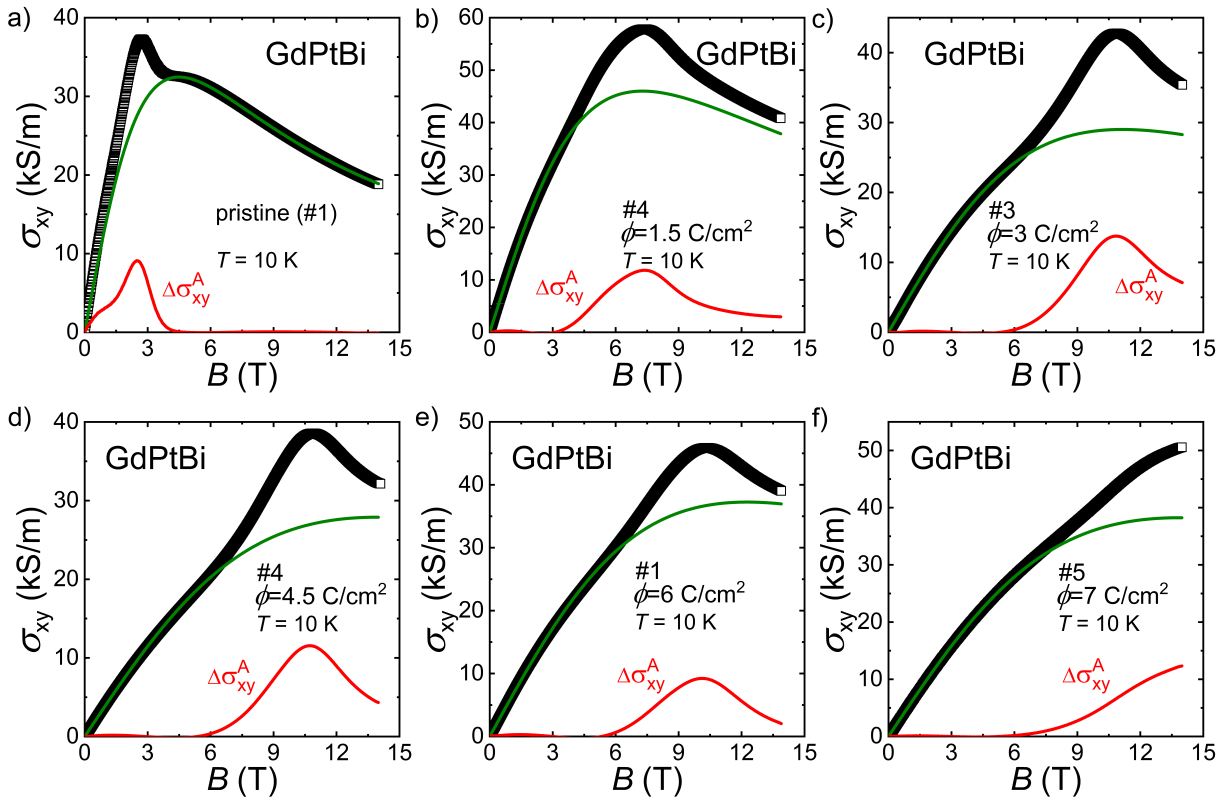


FIG. S6. Separation of anomalous Hall contribution using the Drude model. Magnetic field dependence of Hall conductivity measured at  $T = 10$  K (blue line), theoretical curved generated using the fitting parameters obtained from the Drude model fit (olive line) and their difference (red line) for pristine sample #1 (a), sample irradiated with  $\phi = 1.5 \text{ C/cm}^2$  (b),  $\phi = 3 \text{ C/cm}^2$  (c),  $\phi = 4.5 \text{ C/cm}^2$  (d),  $\phi = 6 \text{ C/cm}^2$  (e) and  $\phi = 7 \text{ C/cm}^2$  (f).

The magnetic field dependence of AHC of all the samples studied is shown in Fig. S7a. To compare the parameters obtained by both approaches of AHE extraction (Drude model fitting and

direct subtraction), we plotted them together on a single plot. The irradiation dose dependences of  $B_{max}$  (the magnetic field at which AHC attains its maximum value for a particular sample) and the maximum value of AHC are shown in Fig. S7b and Fig. S7c, respectively. Fig. S7 demonstrates that  $B_{max}(\phi)$  curves show a negligible difference. In contrast, the values of  $\Delta\sigma_{xy}^A$  obtained using the Drude model fitting are smaller than the values extracted by the subtraction of two experimental curves recorded at 10 K and 50 K (method of AHE extraction, results of which are presented in the main text), but are of the same order of magnitude.

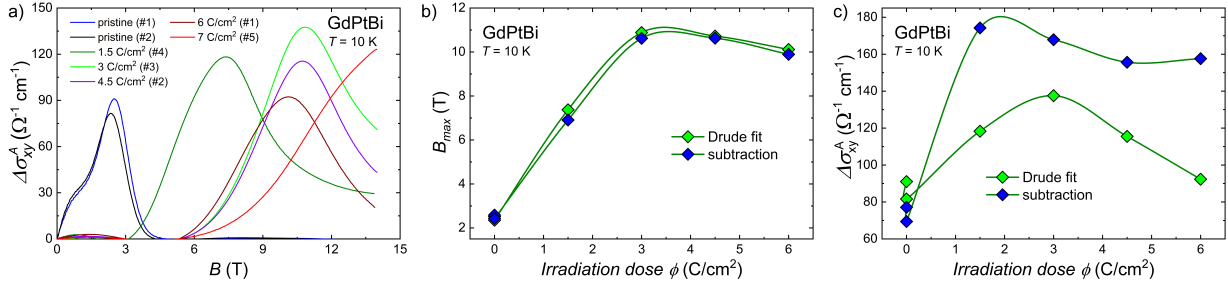


FIG. S7. (a) Anomalous Hall conductivity extracted using the Drude model as a function of magnetic field at  $T = 10$  K for pristine and irradiated samples. (b) The magnetic field values at which AHC reaches its maximum as a function of the irradiation dose at  $T = 10$  K. (b) The maximum values of AHC as a function of the irradiation dose at  $T = 10$  K. In panels (b) and (c), green and blue diamonds correspond to the values extracted using methods based on the Drude model fitting and subtraction of experimental curves measured at  $T = 50$  K from that measured at  $T = 10$  K, respectively.

### Anomalous Hall effect as a function of magnetization

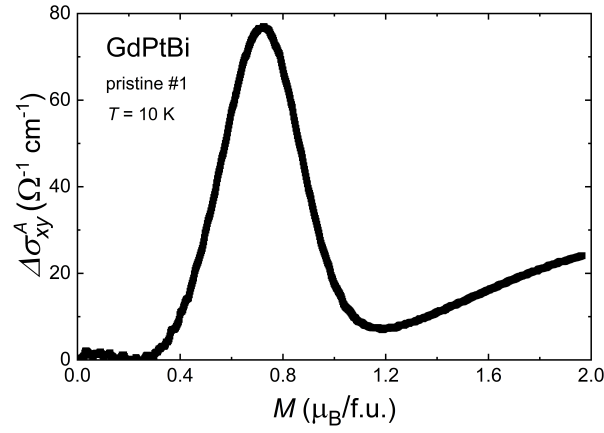


FIG. S8. Anomalous Hall conductivity extracted using methods based on the subtraction of experimental curves measured at  $T = 50 \text{ K}$  from that measured at  $T = 10 \text{ K}$  plotted as a function of magnetization measured at  $T = 10 \text{ K}$  for pristine sample of GdPtBi.

### Calculated cross-sections for Frenkel pair production

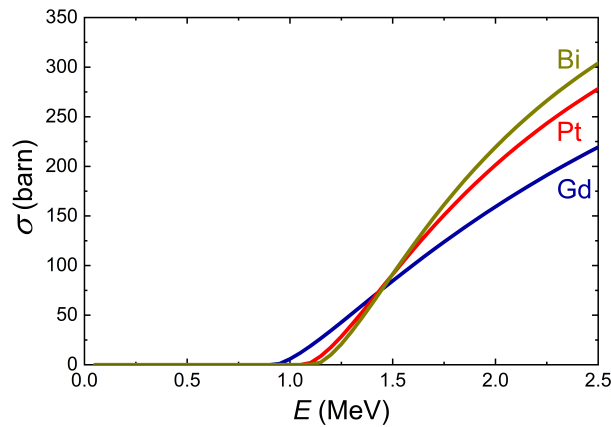


FIG. S9. Frenkel pair production cross-sections ( $\sigma$ ) for Gd, Pt and Bi sublattices as a function of electron energy ( $E$ ).

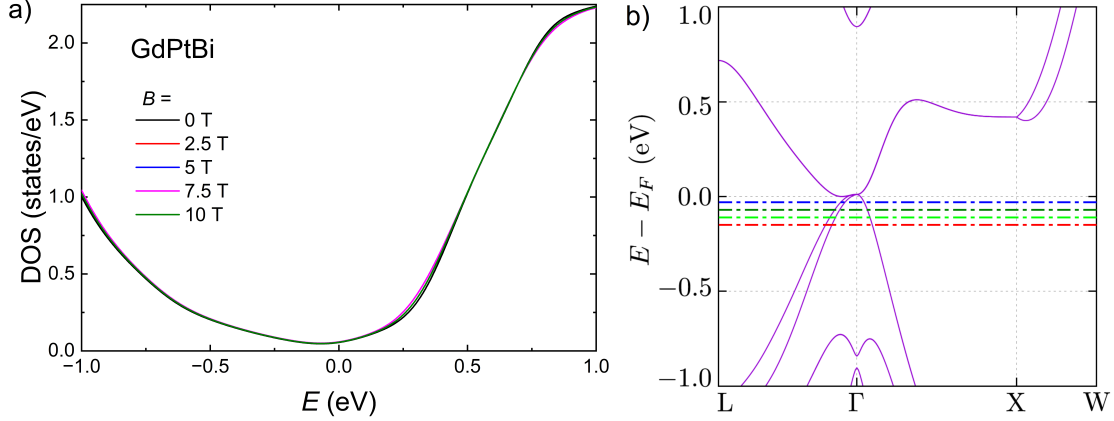


FIG. S10. (a) Density of states as a function of energy for several different values of magnetic field; (b) Calculated electronic band structure in the absence of magnetic field. The horizontal blue, olive, green and red dashed lines correspond to Fermi levels obtained from the Hall carrier concentrations in the pristine, 1.5, 3, and 7 C/cm<sup>2</sup> irradiated samples, respectively.

### Determination of the Fermi level position in the studied samples

There is slight difference in the density of states calculated for zero magnetic field and for several different values of the magnetic field in the range 2.5-10 T (see Fig.S10a). Therefore, we used the results of electronic structure calculations obtained for zero magnetic field to determine the position of the Fermi level in the studied samples. Using the value of the Fermi wave vector  $k_F$  calculated for  $\Gamma - X$  high symmetry line for different values of energies, we calculated the carrier concentration using the formula  $n = V_F/(4\pi^3)$ , where  $V_F$  is volume of the Fermi pocket, which we assumed to be a sphere. By comparing the theoretically calculated carrier concentrations with those determined experimentally from the Hall effect data, we estimated the position of Fermi level in pristine and irradiated samples, as depicted schematically in Fig. S10b.

### Magnetic susceptibility of pristine and irradiated samples

To provide further evidence for the existence of antiferromagnetic order in the studied samples, we performed measurements of magnetic susceptibility,  $\chi$ , as a function of temperature. We measured pristine sample, which was cut from the same crystal as all samples that were irradiated. We also measured the magnetic susceptibility of the sample #5, which was irradiated with the highest dose of 7 C/cm<sup>2</sup>. These measurements confirmed the presence of clear anoma-

lies associated with antiferromagnetic ordering at  $T_N \approx 9\text{ K}$  (see Fig. S11). It should be also noted that in the magnetic susceptibility data of the pristine sample, an upturn was observed at low temperatures, which can be attributed to the presence of a small paramagnetic impurity. Previously, similar behavior in  $\chi(T)$  data was reported by different groups for GdPtBi[S8, S9]. Interestingly, in the irradiated sample, this contribution from the paramagnetic impurity becomes more pronounced (see Fig. S11).

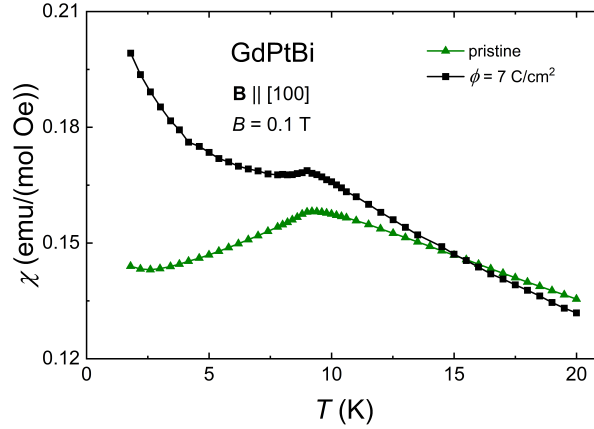


FIG. S11. Temperature dependence of magnetic susceptibility of pristine sample and sample irradiated with  $7\text{ C/cm}^2$  dose. Measurements were done in magnetic field of  $0.1\text{ T}$  applied parallel to  $[100]$  crystallographic direction.

- 
- [S1] Zhu, Y. *et al.* Large anomalous Hall effect and negative magnetoresistance in half-topological semimetals. *Commun. Phys.* **6**, 346 (2023). URL <https://doi.org/10.1038/s42005-023-01469-6>.
- [S2] Shekhar, C. *et al.* Anomalous Hall effect in Weyl semimetal half-Heusler compounds RPtBi (R = Gd and Nd). *Proc. Natl. Acad. Sci. U.S.A.* **115**, 9140 (2018). URL <https://doi.org/10.1073/pnas.1810842115>.
- [S3] Suzuki, T. *et al.* Large anomalous Hall effect in a half-Heusler antiferromagnet. *Nat. Phys.* **12**, 1119 (2016). URL <https://doi.org/10.1038/nphys3831>.
- [S4] Pavlosiuk, O., Fałat, P., Kaczorowski, D. & Wiśniewski, P. Anomalous Hall effect and negative longitudinal magnetoresistance in half-Heusler topological semimetal candidates TbPtBi and HoPtBi. *APL Mater.* **8**, 111107 (2020). URL <https://doi.org/10.1063/5.0026956>.

- [S5] Zhu, Y. *et al.* Exceptionally large anomalous hall effect due to anticrossing of spin-split bands in the antiferromagnetic half-Heusler compound TbPtBi. *Phys. Rev. B* **101**, 161105 (2020). URL <https://doi.org/10.1103/PhysRevB.101.161105>.
- [S6] Chen, J. *et al.* Large anomalous Hall angle accompanying the sign change of anomalous Hall conductance in the topological half-Heusler compound HoPtBi. *Phys. Rev. B* **103**, 144425 (2021). URL <https://doi.org/10.1103/physrevb.103.144425>.
- [S7] Singha, R., Roy, S., Pariari, A., Satpati, B. & Mandal, P. Magnetotransport properties and giant anomalous Hall angle in the half-Heusler compound TbPtBi. *Phys. Rev. B* **99**, 035110 (2019). URL <https://doi.org/10.1103/PhysRevB.99.035110>.
- [S8] Schindler, C. *et al.* Anisotropic electrical and thermal magnetotransport in the magnetic semimetal GdPtBi. *Phys. Rev. B* **101**, 125119 (2020). URL <https://doi.org/10.1103/PhysRevB.101.125119>.
- [S9] Hirschberger, M. *PhD thesis: Quasiparticle Excitations with Berry Curvature in Insulating Magnets and Weyl Semimetals* (Princeton University Press, Princeton, 2017). URL <http://arks.princeton.edu/ark:/88435/dsp010c483n033>.